ELSEVIER

Chemical Engineering Journal 70 (1998) 105–113

Chemical Engineering Journal

Fluid dynamics of bubble columns at elevated temperature modelling and investigation with refractive fiber optic sensors

J. Chabot [a], H. Farag [b], H. de Lasa [b,*]

[a] *Chevron Research and Technology, Richmond, CA, USA*

[b] *Chemical Reactor Engineering Centre, University of Western Ontario, London, Ontario, Canada N6A 5B9*

Received 27 May 1996; revised 27 February 1997; accepted 2 January 1998

Abstract

Experiments are performed in a bubble column using refractive fiber optic sensors and a paraffinic oil. A temperature range of 100–175°C is considered for the study. A two-dimensional fluid recirculation model is applied and this allows the successfully representation of the experimental bubble rise velocity in the bottom section of the column and the confirmation that in the peripheral region of the column, there is important gas recirculation. Valuable insights concerning the turbulent kinematic viscosity, a key model parameter, are reported. Other important effects such as the influence of temperature, gas superficial velocity and axial position on the turbulent kinematic viscosity are also described.

Keywords: Fluid dynamics; Bubble columns; Refractive fiber optic sensors

1. Introduction

The design, scale-up and operation of bubble and slurry bubble columns requires thorough understanding of the fluid dynamics of these systems. Recent technical literature approaches the study of bubble columns using numerical simulation [1,2] and this with the help of the extensive data reported for air–water systems.

Many systems of practical interest (e.g., methanol synthesis reactor using a paraffinic oil) involve, however, hydrocarbon media and elevated temperatures and for these systems very limited information is available. Measured data are, thus, compulsory for validation of underlying models for these systems [3].

Phase recirculation is commonly encountered in bubble columns. The bubbles rising in a liquid media entrain in their evolution liquid upwards. Because of continuity, an equal amount of liquid must therefore flow downwards. Thus, a circulation pattern is driven by the density difference between the gas and liquid and it arises due to radially non-uniform gas hold-up profiles.

The scale of the macroscopic liquid circulation depends on bubble flow regime. For a heterogeneous distribution of bubbles in which the gas transport preferentially takes place in the form of fast-rising large bubbles, high circulation rates occur in the liquid phase.

It has to be mentioned that the effects, however, of column size, distributor and internals design, physical properties of the two-phase system and of the operating conditions on liquid recirculation are still not well-understood.

Prediction of liquid recirculation based on an early inviscid pressure balance model [4] is limited to shallow tanks stirred with gas plumes, and low gas superficial velocities ($V_g \approx 1$ cm/s). The laminar liquid circulation and 'bubble street model' [5] based on pressure balance, for liquids were found to deviate as the liquid viscosity decreased, or as the liquid flow became turbulent.

In commercial columns of practical interest, the liquid flow is turbulent and the theory of laminar circulation is limited to small diameter columns and/or highly viscous liquids. In this respect, Bhavaraju et al. [6] analyzed the problem of laminar and turbulent liquid circulation and developed a model based on multiple cells in the transverse direction. Since experimental measurements of the liquid velocity indicated, however, the absence of multiple cells in the transverse direction, this model was unable to adequately predict the liquid velocity.

Whalley and Davidson [7] proposed an energy balance method to predict the liquid recirculation in shallow bubble columns ($H/D_c \approx 1$). This model was proven unsuccessful

* Corresponding author.

1385-8947/98/$19.00
PII S1385-8947(98)00075-8

in taller bubble column systems [8] and thereafter, it was modified using the so-called principle of minimization of maximum vorticity. However, the application of the single phase vorticity transport equations to two phase flow led to the questionable prediction of multiple circulation cells of height equal to column diameter.

However, since it is indeed physically impossible for streamlines of adjacent cells to oppose each other [9], this model was modified [10]. The modified model, however, predicts that axial centerline velocity alternates in direction along the column which is contrary to experimental observations. Moreover, in such a flow patterns, inter-cell interaction is minimal and hence, significant inter-cell concentration and temperature gradients can develop which has never been experimentally observed. No evidence that these cells are actually fixed in space [11], was so far, presented. It seems likely, according to Dudukovic and Devanathan [11] that these liquid circulation cells consist of travelling secondary vortices, superimposed over the classical macroscopic liquid circulation pattern. Experimental confirmation of such macroscopic liquid circulation pattern was indeed provided by a number of authors [11–17].

As stated, fluid dynamic data of bubble columns operated with hydrocarbon media and at elevated temperatures is quite limited [18]. Fluid dynamic data with concurrently evaluation of both gas hold-up and bubble velocities is even scarcer [12,19]. It is the goal of the present study, with the help of fluid dynamic data obtained by the means of fiber optic refractive sensors, to attempt the evaluation of a turbulent circulating flow model.

2. Theoretical background

Ueyama and Miyauchi [14] and Miyauchico and Shyu [20] developed a turbulent circulating flow model, based on pressure balance. The equation of motion assuming no end effects and constant radial pressure is as follows:

$$\frac{-1}{r}\frac{\mathrm{d}}{\mathrm{d}r}(r\tau_s)=\frac{\mathrm{d}p}{\mathrm{d}z}+(1-\epsilon_{g,loc})\rho_l g \tag{1}$$

Eq. (1) represents the momentum balance of the mixture and τ_s the shear of the mixture. The incorporation of τ_s is required given Eq. (1) is the result of an averaging process of the Navier–Stokes equation where two types of fluctuating velocity terms are involved: independent of and dependent of bubble agitation [21]. This gives rise while averaging the Navier–Stokes equation to averages of non-zero products of fluctuating liquid velocities. The shear stress τ_s accounts for these terms and is defined through the turbulent kinematic viscosity, while the molecular kinematic viscosity is assumed, with the only exception of the near wall region, to be negligible.

$$\tau_s=-\nu_t\rho_l\frac{\mathrm{d}U_l}{\mathrm{d}r} \tag{2}$$

Different constitutive relations have been proposed for the eddy viscosity, ranging from purely empirical correlations, as reviewed by Deckwer and Schumpe [22], to models based on turbulence single phase mixing length [23] and von Karman's hypothesis [24].

Two boundary conditions can be considered to solve Eq. (1). One of these boundary conditions assumes axi-symmetric liquid flow in the column:

$$\frac{\mathrm{d}U_l}{\mathrm{d}r}=0 \text{ at } r=0 \tag{3}$$

This applies in the current study given the gas distribution system provided both the appropriate pressure drop and distribution of openings throughout the cross-section of the column. Both these conditions were met under all the operating conditions investigated and axi-symmetric gas flow at the distributor level was safely assumed. Note that pressure drop for all operating conditions were at least 30% of the pressure drop in the bed. In addition, the vertical alignment of the column was carefully verified using precise level measurements, thus insuring axi-symmetrical circulation flow patterns in the system.

A second boundary condition is obtained from the 'Universal Velocity Distribution for Turbulent Flow' [14]. This boundary condition assumes that the laminar sublayer can be neglected and hypothesizes a logarithmic liquid velocity profile close to the wall [25]. As a result the velocity at the wall is equal to $U_{l,w}$:

$$U_{l,w}=-11.63\frac{\sqrt{|\tau_w|}}{\rho_l} \tag{4}$$

For uniformly distributed rising bubbles in a batch system (no net liquid circulation), the relationship between the mean gas holdup ($\epsilon_{g,avg}$) and the slip velocity of the bubbles relative to the liquid, V_{slip}, is given by:

$$\frac{V_g}{\epsilon_{g,avg}}=V_{slip} \tag{5}$$

Regarding the batch operation for the liquid, this was a sound assumption given the unit used was equipped with a water reflux condenser filled with stainless steel balls in the lower section. Then, and in spite of the relatively high hydrocarbon vapour pressure and significant liquid droplets entrainment, there were no losses of liquid. Liquid level remained constant during the experimental program.

Ueyama and Miyauchi [14] prefer, however, the following relationship to relate the slip velocity of the gas bubbles to the gas superficial velocity in the circulation flow regime (batch system):

$$V_{slip}=\frac{V_g}{\epsilon_{g,avg}}-\frac{1}{(1-\epsilon_{g,avg})}\left(\frac{U_{l,c}-U_{l,w}}{(m+4)}\right) \tag{6}$$

Constant slip velocity is a reasonable assumption. Such an assumption was experimentally validated by a number of authors [14,26,25]. This can be supported given the close

dependence of the slip velocity on bubble sizes. In the present study, bubble sizes changed following a log-normal distribution [19] and the average bubble sizes were subject to moderate variations only. For example, the changes observed for average bubble sizes were as follows: from 2.5 mm at $r/R=0.92$ to 4.3 mm at $r/R=0.19$. Thus, there is a relatively small variation of the average bubble chords. Furthermore, considering the postulated slip velocity relationship involving the square root of the characteristic dimension [14], an extreme 26% change of the slip velocity across the reactor section can be expected. This supports the model assumption of a uniform slip velocity across the reactor section.

Moreover, an expression for the radial profile of the gas holdup, as reported by Chabot and de Lasa [19]:

$$\epsilon_{g,loc}(\theta)=\epsilon_{g,avg}\left(\frac{m+2}{m}\right)(1-\theta^n) \tag{7}$$

can be adopted with the m adjusted for every axial level and experimental condition. It was shown in this contribution that the m values were quite high changing between 4 and 24. A marked change of this parameter was also observed between the lower position $z=15$ cm and the other levels studied $z\geq 30$ cm. It was judged this change corresponded to the emergence or development of the parabolic gas hold-up profile. At higher positions, however, it was found that m became a weaker function of the axial position. The m parameter was also found to be influenced by gas superficial velocity and this dependence was particularly significant at gas superficial velocities smaller than 9 cm/s. Temperature increase in the 100°C to 175°C range increased on the average m by 35%.

Furthermore, concerning the turbulent kinematic viscosity is considered a constant parameter [11]. This is a sound assumption considering that bubble fractions were above 3% and as a result there was a dominant contribution of the bubble induced turbulence on the turbulence viscosity [27]. Under these conditions, ν_t is strongly influenced by slip velocity and given the slip velocity does not change significantly in the radial direction this parameter can be considered a constant/cuasi-constant parameter.

On the basis of these hypothesis, the following expressions for the liquid velocity are obtained:

$$U_{l,w}=-(11.63)^2\frac{\nu_t J_1}{R}\left(-1+\sqrt{1+\frac{\left(2J_0-\left(\frac{\epsilon_{g,avg}}{2}\right)\right)}{(11.63)^2 J_1^2}\frac{R^3 g}{\nu_t^2}}\right) \tag{8}$$

and:

$$U_l=U_{l,w}+\frac{R^2}{\nu_t}\left[\left(\frac{\tau_w}{2R\rho_l}+\frac{\epsilon_{g,av}g}{2m}\right)(1-\theta^2)-\frac{\epsilon_{g,av}g}{m(m+2)}(1-\theta^{m+2})\right] \tag{9}$$

where:

$$J_0=\frac{(m+6)\epsilon_{g,avg}}{4(m+4)}\frac{1-\frac{(m^2+10m+20)}{(m+2)(m+6)}\epsilon_{g,avg}}{1-\frac{(m+6)}{(m+4)}\epsilon_{g,avg}} \tag{10}$$

$$J_1=\frac{2(1-\epsilon_{g,avg})}{1-\frac{(m+6)}{(m+4)}\epsilon_{g,avg}} \tag{11}$$

3. Experimental procedure

The design of the fibre optic sensor, used in the present study, was based on the difference of refractive index between the gas phase and the liquid phase. According to Snell's law, the angle of total reflection is larger in the liquid than in the gas phase. If this principle applies to a fibre optic having a U-shape, the fibre has to be bent such as the radius of curvature of the U has to be large enough so that the angle of incidence of the light at the turning point is greater than the angle of total reflection when the same fibre is exposed to a gas phase. If this condition is met, the source light is conserved in the fibre and light can be detected at the extremity of the detection fibre. However, the radius of curvature of the U-shape fibre has to be, at the same time, curved in such a way that the radius is small enough to secure an angle of incidence at the turning point smaller than the angle of total reflection for the same fibre exposed to the liquid phase. Therefore, a significant fraction of the source light is lost at the turning point and only a small light intensity is observed at the end of the detection fibre. Then, substantial differences in the detected light can be observed depending on the phase present (gas or liquid) at the fiber turning point (detecting tip). Thus, if such fibre is properly inserted at a given position in a bubble column or a slurry bubble column, local real-time discrimination between the gas phase (gas bubbles) and the liquid phase can be achieved. Individual gas bubbles, as they contact the detecting tip of the fibre optic sensor can be tracked.

In the present study, fibre optic sensors consisted of an incident fibre optic connected to a detecting fibre optic via a sharp U-shape turning point. In order to optimize the use of the two optical sensors, the insertion angle of the optical sensors detecting tips was at a 45° pointing downward to ensure optimum and equal visibility of both, ascending and descending bubbles [12]. (Fig. 1)

Two optical sensors, mounted on individual HTX-13 tubing, were attached to a single 1/4″ tubing, which was soldered to a solid metallic bloc. The two optical sensors had their respective detecting tips separated by a vertical distance of 0.5 cm and were pointing downward with a 45° angle with respect to the vertical position. The solid metallic block could then be attached to a specially designed insertion system.

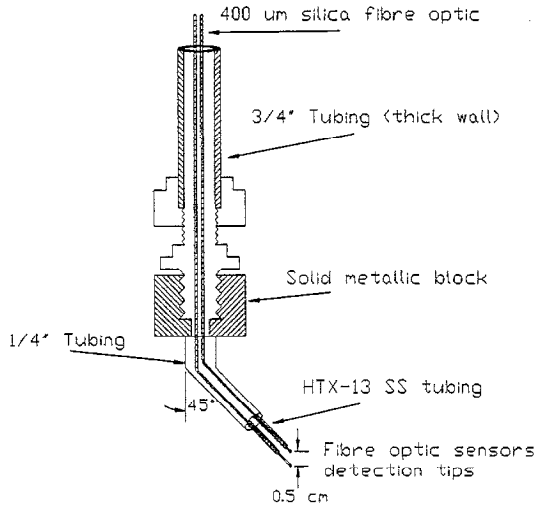

Fig. 1. Description of the refractive fibre optic sensors angled at 45°.

This 'periscopic' system consisted of a 2.75-m long, 0.0191-m diameter stainless steel tube. This tube was inserted into the column through the top flange of the column, in a median point between the center of the column and the wall of the column. The system was designed in such a way that when performing a 180° rotation of the long vertical tube, the detecting tips of the two sensors were displaced from the vicinity of the center to the vicinity of the column wall (Fig. 2). The detecting tips of the sensors could also be displaced axially by moving the insertion tube up or down. The long vertical tube then served the purpose of both controlling the axial and radial positions of the detecting tips of the sensors, while serving as a protection chamber for the incident and detecting fibres. Consequently, the four fibre optics (two incident and two detecting fibres) were isolated from the column environment and were protected during displacement of the insertion system. As shown in Fig. 2, several radial positions were investigated with precision of approximately ± 1 mm. Additional details about the various components of the fiber optic sensors, the photoelectronic system and the data acquisition system are given in Ref. [12].

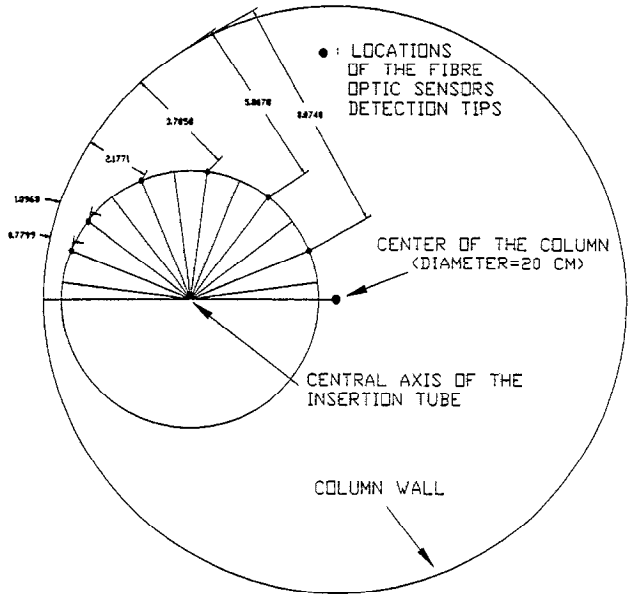

Fig. 2. Radial position of fibre optic sensors using the insertion system.

The experiments were conducted at atmospheric pressure and at temperatures in the 100–175°C range in a 0.2-m diameter and 2.4-m height carbon steel column. A commercial paraffinic oil was employed as the liquid phase while nitrogen was used as the gas phase [12].

The measurement of the local gas phase characteristics (gas hold up, bubble rise velocity, bubble chord length and bubble chord length distribution) was performed at six different radial positions ($r/R = 0.19$, 0.42, 0.62, 0.78, 0.89, 0.92) and several axial positions (from 15 to 76 cm above the gas distributor), using refractive optical sensors [28], coupled with a periscopic sensors insertion system [19]. Typical examples of these measurements for gas hold-up and bubble chord are provided in Figs. 3 and 4.

The gas was introduced into the column via a perforated plate distributor consisting of 40 holes (1.59 mm diameter) arranged in a triangular pitch (2.8 cm). Additional details about the specific configuration of the distributor used are reported by Chabot [12] and Chabot and de Lasa [19]. The gas superficial velocity was varied throughout the experiments between 2.2 and 14.7 cm/s.

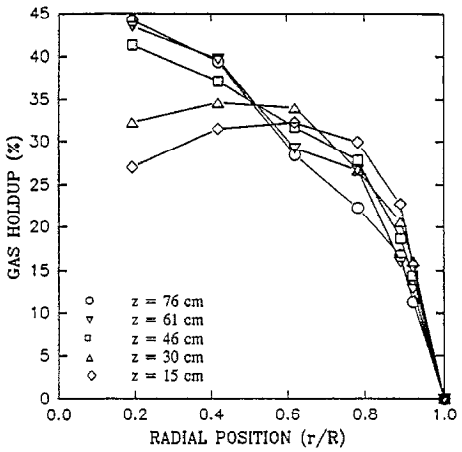

Fig. 3. Change of gas holdup with r/R at $T = 175$°C and $V_g = 14.7$ cm/s.

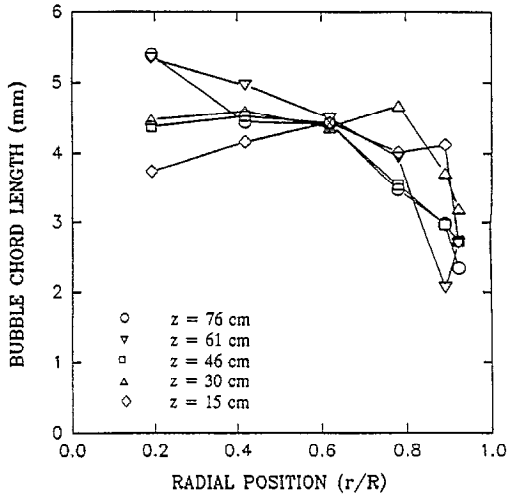

Fig. 4. Change of bubble chord length with r/R at $T = 175$°C and $V_g = 14.7$ cm/s.

4. Data analysis

The first step in the data analysis was the performance of the gas mass balance. These gas mass balances were developed at both $z=30$ cm and $z=76$ cm. Note that the ability of the fibre optic sensor to measure both local bubble rise velocity and local gas hold up provides the possibility of calculating $V_{g,measured}$. For a given axial position, a cross-sectional average gas superficial velocity can be evaluated using the following expression:

$$V_{g,measured}=\frac{1}{\pi R^2}\int_0^R V_{b,loc}\,\epsilon_{g,loc}\,2\pi r dr \quad (12)$$

where $V_{g,measured}$ is the cross-sectional average gas superficial velocity, $V_{b,loc}$ is the local average bubble rise velocity measured by the optical sensors, and $\epsilon_{g,loc}$ is the local gas hold-up value also obtained (measured) from the fibre optic measurements.

The previous equation implies, of course, that all the gas present at a given location ($\epsilon_{g,loc}$) rises with an average velocity $V_{b,loc}$. Since, the individual bubble rise velocity distributions observed were relatively wide (the gas present at a given location was actually rising with a wide distribution of velocities) and to verify that such phenomenon was not introducing undue imprecisions in the gas mass balance, the gas hold-up and the individual bubble rise velocity distribution were used to perform gas mass balances. This allowed to confirm that using, for given radial position, time average quantities ($\epsilon_{g,loc}$, $V_{b,loc}$) did not introduce significant errors. Errors were never in excess to 5%. Moreover, the above equation is based on the assumption of axi-symmetric in the radial direction. This assumption thus requires an effective gas distribution system providing both the appropriate pressure drop and an axi-symmetric distribution of openings throughout the cross-section of the column. Both these conditions were met in the present study under all the operating conditions investigated. In addition, the vertical alignment of the column was carefully verified using precise level measurements, thus, insuring symmetric circulation flow patterns in the system.

The superficial gas velocity obtained from the above equation, $V_{g,measured}$ was compared to the actual gas superficial velocity, taking special care to correct the former one for any pressure and/or vapour pressure effects:

$$\frac{[V_{g,measured}-V_{g,fed}]}{V_{g,fed}}\times 100 \quad (13)$$

It was found, as reported by Chabot [12], that differences of the mass balance closed fairly well at $z=30$ cm. Typical deviations were inside 10% and this was observed at both 100°C and 175°C. Deviations were, however, much higher at $z=76$ cm, and this discrepancy was the result of overestimation of the bubble gas velocity ($V_{b,measured}$).

The adjustment of the kinematic viscosity was developed minimizing the following relationship:

$$\Sigma(G_{model}-G_{fed})^2=\text{minimum} \quad (14)$$

with G_{fed} (mass gas flow $=V_{g,fed}\,\pi R^2$) based on the gas fed to the unit and G_{model} (mass gas flow) defined as:

$$G_{model}=\int_0^R V_{b,model}\,\epsilon_{g,model}2\pi r dr \quad (15)$$

Thus, adjustments of the G_{model} through changes of the ν_t using a Marquart–Levenberg algorithm, yielded optimized ν_t values (2% deviations). The objective function was based on providing a closure of the gas mass balance as good as possible. With these values $V_{b,model}$ were obtained. Differences between $V_{b,measured}$ and $V_{b,model}$, as shown in Figs. 6–8 for $z=76$ cm, reflect essentially discrepancies between G_{fed} or G_{model} with respect to $G_{measured}$. In this respect, the enclosed Table 1 provides a quick visualization of calculations and superficial gas velocities employed. Case 1 uses $V_{g,measured}$ and $V_{g,fed}$ and Case 2 uses $V_{g,model}$ and $V_{g,fed}$. Thus, the proposed methodology provides $V_{b,model}$ and $V_{b,measured}$ parameters calculated independently. Consequently, the proposed methodology represents a true test of the validity of the proposed model through comparison of $V_{b,model}$ and $V_{b,measured}$.

5. Results and discussion

Application of the model, given by Eqs. (6)–(11) requires two parameters, namely the gas hold-up radial profile and the turbulent kinematic viscosity. Since precise and validated measurements of the gas hold-up radial profiles were effected [12,19], the m parameter involved in Eq. (7) is available. Thus, the model considered is, in practice, a one-parameter model, with the turbulent kinematic viscosity being the single unknown parameter to be calculated by numerical regression.

About the turbulent kinematic viscosity in two-phase bubble column system, limited information only, is available [14,22,26]. Furthermore, correlations developed mostly for air–water systems to predict the turbulent kinematic viscosity,

Table 1
Summary of parameter calculations

Superficial gas velocity involved, $V_{g,i}$	Case 1: Checking of the gas mass balances	Case 2: Calculation of the kinematic viscosity by regression
$V_{g,fed}=G_{fed}/(\pi R^2)$	1	1
$V_{g,measured}=G_{measured}/(\pi R^2)$	1	0
$V_{g,model}=G_{model}/(\pi R^2)$	0	1

1 represents parameter included, 0 represents parameter not included.

may not provide reliable estimates of the turbulent kinematic viscosity under the present operating conditions.

As described above, the calculation of ν_t involved a regression analysis (refer to Table 1). Once this numerical regression is completed, the liquid velocity (U_l) was calculated using Eqs. (6) and (9), respectively, and the bubble slip velocity employing Eq. (12). So, the bubble velocity was given as:

$$V_{b,model} = V_{slip} + U_l \quad (16)$$

The calculated liquid velocity and bubble velocity radial profiles, obtained for several of the gas superficial velocities studied, using the above described procedure, are presented in Figs. 5–8 for $T = 100°C$. As shown in Figs. 6–8, the correspondence between calculated velocity and measured bubble rise velocity is very good, being within 10%, for $V_g = 4.1$ to 14.7 cm/s, and $z = 30$ cm. These results confirm the following: (a) the validity of the experimentally measured bubble rise velocities ($V_{b,measured}$) given the appropriate closure of the overall gas mass balance, (b) the applicability of the selected model for these operating conditions and axial position studied.

Good agreement in the central section and a poor correspondence in the outer column section, between the predicted and measured gas velocities was, however, observed at $z = 30$ cm and $V_g = 2.2$ cm/s (Fig. 7). It has to be mentioned that this discrepancy between $V_{b,model}$ and $V_{b,measured}$ takes place under the constrains of an overestimated $V_{g,measured}$ or an overestimated measured mass balance by 28%. As described in Table 1, the mass balance for the model is established on the basis of $V_{g,fed}$ and the $V_{b,model}$ profile obtained in this way yields, in the peripheral area, smaller velocities than the ones measured with the fiber optic sensor. Thus, discrepancy between $V_{b,measured}$ and $V_{b,model}$ in the column peripheral section is coming together with a deficiency in the mass balance (Eq. (13)). This reflects the weakness of the fiber optic sensor and the associated data analysis to properly assess the net bubble flow. While this is, in a sense, an obstacle for bubble column modelling in the outer section, this is helpful as well, because it points towards the existence of a secondary liquid circulation cell (upward liquid flow along the wall of the column, downward liquid flow in the central region of the column).

Moreover, as shown in Figs. 5 and 8, for $z = 76$ cm, the measured bubble rise velocities are consistently higher than the model velocities resulting form Eq. (13). This is true again in the peripheral column region and this confirms the presence of strong gas bubble backmixing at the higher column levels.

It has to be stressed, however, that for all the conditions studied, excellent correspondence is observed between the measured bubble rise velocities and the calculated ones in the central section of the column ($\Theta = 0.19$), where bubble recirculation is minimum, as confirmed by Yao et al. [29]. On average, for all the gas superficial velocities studied, the discrepancy between calculated and measured bubble velocities

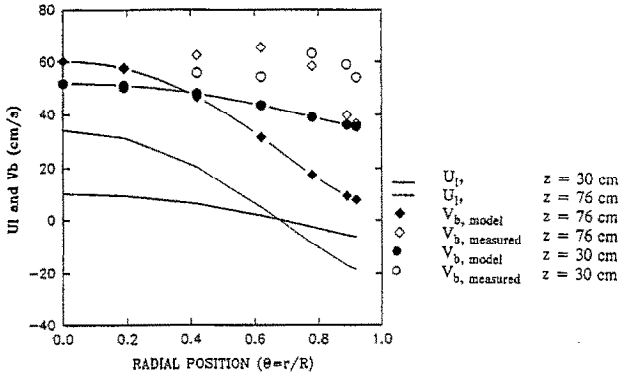

Fig. 5. Calculated U_l, V_b and experimental V_b values for $T = 100°C$ and $V_g = 2.2$ cm/s.

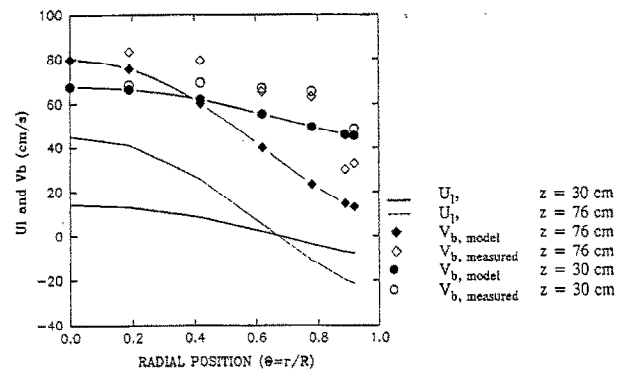

Fig. 6. Calculated U_l, V_b and experimental V_b values for $T = 100°C$ and $V_g = 4.1$ cm/s.

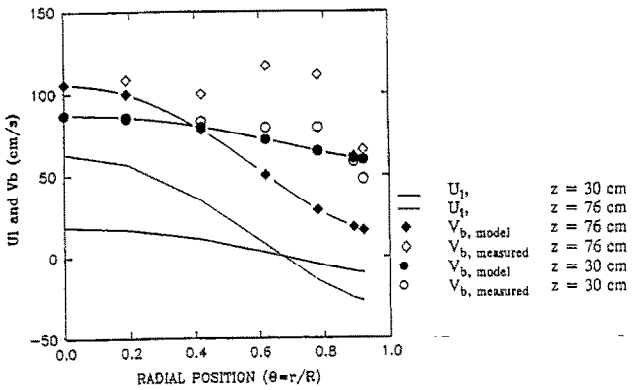

Fig. 7. Calculated U_l, V_b and experimental V_b values for $T = 100°C$ and $V_g = 9.0$ cm/s.

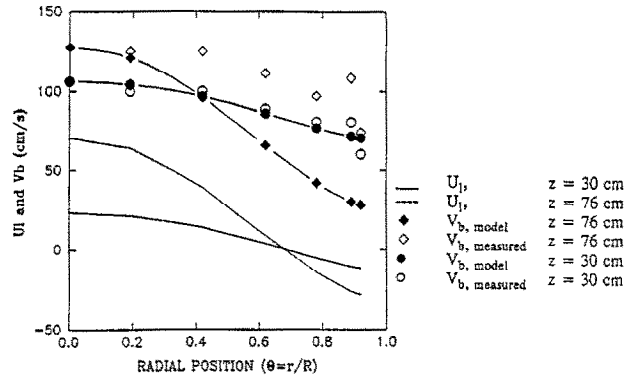

Fig. 8. Calculated U_l, V_b and experimental V_b values for $T = 100°C$ and $V_g = 14.7$ cm/s.

is equal to 5.7% for $\Theta = 0.19$, $z = 76$ cm and $T = 100$°C. This further confirms the validity of the measured bubble rise velocities. On this basis, the occurrence of gas backmixing is found to gradually increase from the bottom of the column to the top of the column as the liquid circulation flow is fully established. In this respect, it is valuable to mention that differences between measured bubble rise velocity and net gas velocity in the peripheral region of the column were also reported by Kago et al. [30].

Trends similar to the ones observed at $T = 100$°C are observed at $T = 175$°C. However, in this particular condition, gas backmixing is also observed at the lower axial positions, as a result of both, stronger liquid circulation pattern at the bottom of the column and the presence of smaller bubbles, more likely to be entrained downward. Actually, the liquid circulation flow is observed to develop more quickly at $T = 175$°C, as compared to $T = 100$°C, thus suggesting more complete backmixing of the liquid flow at $T = 175$°C. This is indeed consistent with the results of Ueyama and Miyauchi [14] who did not observe a strong effect of the liquid viscosity under low liquid viscosity conditions (<2 stokes). Under such conditions, these authors claimed that the internal flow of liquid was a fully developed turbulent flow.

The radial average slip velocities obtained, under fully established conditions ($z = 76$ cm), with Eqs. (6)–(11) are presented in Fig. 9. In the liquid circulation regime, the slip velocity augments with an increase of the gas superficial velocity. Furthermore, the slip velocity observed at $T = 175$°C are smaller than the ones observed at $T = 100$°C, since smaller gas bubbles are observed at higher temperature.

As stated, the turbulent kinematic viscosity is optimized, in the present study, to ensure the best possible closure of the gas mass balance (Table 1). The values of the turbulent kinematic viscosity obtained for the fully established liquid circulation regime ($z = 76$ cm) are presented in Fig. 10. While direct comparisons between ν_t are rather difficult, most of the data reported in the technical literature are with water–air media systems, air–water systems show kinematic turbulent viscosities in the 1–2.4 10^{-3} m^2/s range [14]. These ν_t

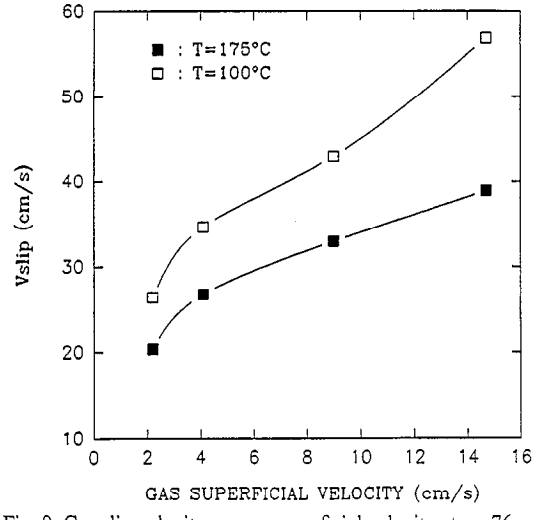

Fig. 9. Gas slip velocity vs. gas superficial velocity at $z = 76$ cm.

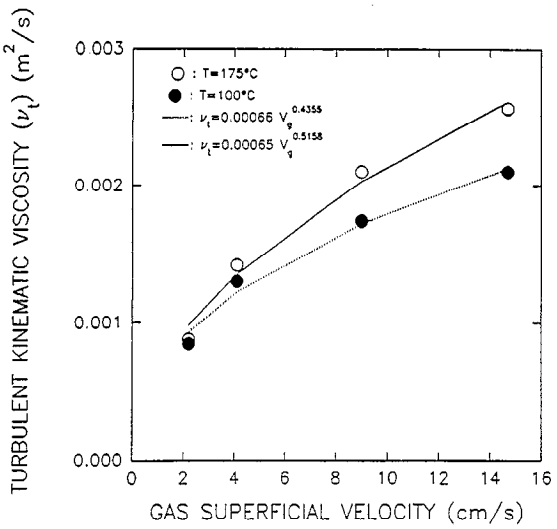

Fig. 10. Turbulent kinematic viscosity vs. gas superficial velocity at $z = 76$ cm.

values are in the same range as the ones obtained in the present study and this appears to be reasonable given there is, in both systems, a dominant induced bubble turbulence effect strongly affected by the slip velocity.

Fig. 10 shows the turbulent kinematic viscosity increase with the gas superficial velocity. The dependence of the turbulent kinematic viscosity on the gas superficial velocity is found to be well-represented by a power law relationship (Fig. 10). Moreover, the turbulent kinematic viscosity as well as the dependence of the turbulent kinematic viscosity on the gas superficial velocity are found to be slightly more pronounced at $T = 175$°C, as compared to $T = 100$°C. The turbulent kinematic viscosity is known to be a function of the eddy scale. As discussed by Rice and Geary [31], the scale of turbulent eddies in two-phase turbulent flow is expected to lie between the bubble average size and the diameter of the column.

Furthermore, it is anticipated that the number population density of bubbles can enhance eddy scaling, becoming larger as bubble concentration (hence, number of interactions) increases [31]. So, as the temperature increases, the bubble size slightly decreases, while the number population density of bubbles augments considerably. As a result, the turbulent kinematic viscosity increase with temperature can be justified.

Similarly, the bubble size and the bubble density are both found to augment with the gas superficial velocity, and, as a consequence, an increase of the turbulent kinematic viscosity is observed. It is interesting to note that, under the conditions investigated in the present study, the dependence of the turbulent kinematic viscosity with the gas superficial velocity is found to be stronger than the one suggested by Miyauchi et al. [32]. However, the values of the turbulent kinematic viscosities observed are found to be, in general, in a similar range than those observed in air–water systems [14].

Furthermore, as shown in Fig. 11, the turbulent kinematic viscosity is a function of the axial position. Thus, the eddy

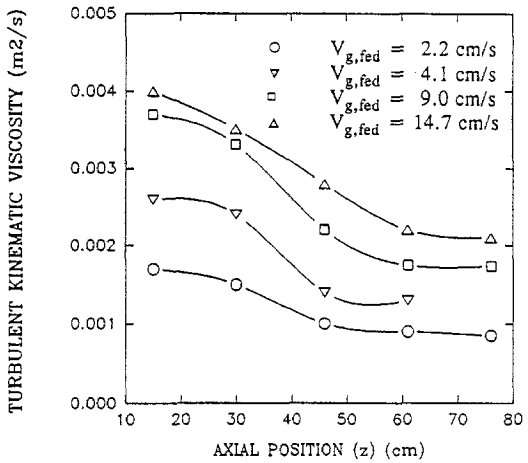

Fig. 11. Turbulent kinematic viscosity vs. axial position at 100°C.

kinematic viscosity is larger at the bottom of the column than at higher axial positions. Regarding the larger turbulent kinematic viscosity observed at the bottom of the column, this is attributed to the characteristic of the flow pattern in this column section yielding bigger slip velocities and consequently higher ν_t values. These effects at the bottom of the column are more pronounced at $T = 100$°C than at $T = 175$°C, which is consistent with the fact that liquid circulation patterns are expected to evolve more rapidly at higher temperatures.

6. Conclusions

Fluid dynamic data of bubble columns operated with hydrocarbon media and at elevated temperatures with concurrently evaluation of both gas hold-up and bubble velocities is very limited. The present study, using fluid dynamic data obtained by means of fiber optic refractive sensors, provides an evaluation of a turbulent circulating flow model.

The ability of this phenomenological based model, originally proposed by Ueyama and Miyauchi [14] and considered as explicitly stated in Eqs. (6)–(11), is found to satisfactorily represent the trend of experimentally measured bubble rise velocities in the bottom section of the column. Discrepancies observed at the higher levels and in the outer column section are attributed to the deficiency of the bubble tracking technique to provide accurate estimations of the net bubble flow.

Moreover, the implementation of this model allows to obtain important insights concerning the influence of the axial position, the gas superficial velocity and elevated temperatures on the turbulent kinematic viscosity in hydrocarbon media.

7. Notation

g	Gravitational acceleration (m^2/s)
G	volumetric flow of gas (m^3/s)
$I(\theta)$	Parameter as given by Eq. (12)
J_0	Parameter as given by Eq. (10)
J_1	Parameter as given by Eq. (11)
m	Parameter in Eq. (7)
p	Pressure (kPa)
r	Radial position (m)
R	Column radius (m)
U_l	Local liquid velocity (m/s)
$U_{l,c}$	Local liquid velocity (center) (m/s)
$U_{l,w}$	Local liquid velocity (wall) (m/s)
V_g	Superficial gas velocity (m/s)
V_b	Bubble rise velocity (m/s)
V_l	Superficial liquid velocity (m/s)
V_{slip}	Bubble slip velocity (m/s)

Greek

ϵ	Holdup
$\epsilon_{g,avg}$	Average radial gas holdup (−)
$\epsilon_{g,loc}$	Local gas holdup (−)
θ	Dimensionless radial position (r/R)
μ_l	Liquid viscosity (kg/(m s))
ρ	Density (kg/m^3)
τ_s	Shear stress
ν_t	Turbulent kinematic viscosity (m^2/s)

Subscripts

fed	Pertaining to the measured data at the unit inlet
g	Gas
l	Liquid
l,c	Relative to liquid in the center
l,w	Relative to liquid close to the wall measured pertaining to the measured data with fiber optic sensors model pertaining to the modelling results
w	At the wall

References

[1] S. Grevskott, B.H. Sannæs, M.P. Dudukovič, K.W. Hjarbo, H.F. Svendsen, Chem. Eng. Sci. 51 (10) (1996) 1703–1713.
[2] A. Sokolichin, G. Eigenberger, Chem. Eng. Sci. 49 (24B) (1994) 5735–5746.
[3] A. Lapin, A. Lübbert, Chem. Eng. Sci. 49 (21) (1994) 3661–3674.
[4] W. Freedman, J.F. Davidson, Trans. Inst. Chem. Eng. 47 (1969) 251–262.
[5] K. Rietema, S.P.P. Ottengraph, Trans. Inst. Chem. Eng. 48 (1970) 54.
[6] S.M. Bhavaraju, T.W.F. Russel, H.W. Blanch, AIChEJ. 24 (3) (1978) 454–466.
[7] P.B. Whalley, J.F. Davidson, Liquid circulation in bubble columns, Proc. Symp. Two Phase Flow System, Inst. Chem. Eng. Symp. Ser., 38 Paper J5 1 (1974).
[8] J.B. Joshi, M.M. Sharma, Trans. Inst. Chem. Eng. 57 (1979) 244–251.
[9] Van Den Akker, K. Rietema, Trans. Inst. Chem. Eng. 60 (1982) 255–256.
[10] J.B. Joshi, M.M. Sharma, Trans. Inst. Chem. Eng. 60 (1982) 255–256.
[11] M.P. Dudukovic, N. Devanathan, Bubble Column Reactors: Some Recent Developments, Proc. Nato-ASI Symp. Ser., Kluwer, E225 (1992) 353.

[12] J. Chabot, Fluid Dynamics of Bubble and Slurry Bubble Columns, PhD Dissertation, University of Western Ontario, London, Ontario, Canada (1993).
[13] J.H. Hills, Trans. Inst. Chem. Eng. 52 (1974) 1.
[14] K. Ueyama, T. Miyauchi, AIChE J. 25 (1979) 258–266.
[15] E. Kojima, H. Unno, Y. Sato, Y. Chida, H. Imai, K. Endo, I. Inoue, J. Kobayashi, H. Kaji, H. Nakanishi, K. Yamamoto, J. Chem. Eng. Jpn. 13 (1) (1980) 16–21.
[16] K. Franz, T. Borner, H.J. Kantorek, R. Buchholz, Ger. Chem. Eng. 7 (1984) 365–374.
[17] B.P. Yao, C. Zheng, H.E. Gasche, H. Hofmann, Chem. Eng. Process, 29 (1991) 65–75.
[18] Z. Renjun, J. Xinzhen, L. Baozhang, Z. Young, Z. Laiqui, Ind. Eng. Res. 27 (1988) 1910–1916.
[19] J. Chabot, H. de Lasa, Ind. Eng. Res. 32 (1993) 2595–2601.
[20] T. Miyauchi, C.N. Shyu, Kagaku Kogaku 34 (1970) 958.
[21] Sekoguchi Sato, J. Multiphase Flow 2 (1985) 79.
[22] W.-D. Deckwer, A. Schumpe, Int. Chem. Eng. 27 (1987) 405–422.
[23] N.N. Clark, C.M. Atkinson, R.L.C. Flemmer, AIChE J. 33 (1987) 575–578.
[24] K.G. Anderson, R.G. Rice, AIChE J. 35 (1989) 514–518.
[25] R. Torvik, H. Svendsen, Chem. Eng. Sci. 45 (1990) 2325–2332.
[26] K. Koide, S. Morooka, K. Ueyama, A. Matsuura, F. Yamashita, S. Iwamoto, Y. Kato, H. Inoue, M. Shigeta, S. Suzuki, T. Akehata, J. Chem. Eng. Jpn. 12 (2) (1979) 98–104.
[27] H.F. Svendsen, H.A. Jakobsen, R. Torvik, Chem. Eng. Sci. 47 (1992) 3297.
[28] J. Chabot, S.L.P. Lee, A. Soria, H. de Lasa, Can. J. Chem. Eng. 70 (1992) 61–68.
[29] B.P. Yao, C. Zheng, H.E. Gasche, H. Hofmann, Chem. Eng. Process, 29 (1991) 65–75.
[30] T. Kago, Y. Sasaki, T. Kondo, S. Morooka, Y. Kato, Chem. Eng. Commun. 75 (1989) 23–38.
[31] R.G. Rice, N.W. Geary, AIChE J. 36 (1990) 1339–1348.
[32] T. Miyauchi, S. Furusaki, S. Morooka, Y. Ikeda, Advances in Chemical Engineering, Vol. 11, Academic Press, New York, 1981, pp. 275–448.